PHYSICAL REVIEW B **95**, 081403(R) (2017)

Spin relaxation 1/f noise in graphene

S. Omar,[1,*] M. H. D. Guimarães,[1,2] A. Kaverzin,[1] B. J. van Wees,[1] and I. J. Vera-Marun[1,3,†]

[1]*The Zernike Institute for Advanced Materials University of Groningen Nijenborgh 4 9747 AG, Groningen, The Netherlands*

[2]*Kavli Institute at Cornell for Nanoscale Science Cornell University, Ithaca, New York 14853, USA*

[3]*School of Physics and Astronomy The University of Manchester, Manchester M13 9PL, United Kingdom*

(Received 15 June 2016; revised manuscript received 12 January 2017; published 7 February 2017)

We report the first measurement of 1/f type noise associated with electronic spin transport, using single layer graphene as a prototypical material with a large and tunable Hooge parameter. We identify the presence of two contributions to the measured spin-dependent noise: contact polarization noise from the ferromagnetic electrodes, which can be filtered out using the cross-correlation method, and the noise originated from the spin relaxation processes. The noise magnitude for spin and charge transport differs by three orders of magnitude, implying different scattering mechanisms for the 1/f fluctuations in the charge and spin transport processes. A modulation of the spin-dependent noise magnitude by changing the spin relaxation length and time indicates that the spin-flip processes dominate the spin-dependent noise.

DOI: 10.1103/PhysRevB.95.081403

Noise in electronic transport is often treated as a nuisance. However, it can have much more information than the average (mean) of the signal and can probe the system dynamics in greater detail than conventional DC measurements [1]. Low frequency fluctuations with a power spectral density (PSD) that depend inversely on frequency, also known as 1/f noise, are commonly observed phenomena in solid state devices. A textbook explanation of the processes generating 1/f noise is given by the McWhorter model where traps are distributed over an energy range, leading to a distribution of characteristic timescales of trapping-detrapping processes of the electrons in the transport channel and causing slow fluctuations in conductivity [2–4].

Graphene is an ideal material for spin transport due to low spin-orbit coupling and small hyperfine interactions [5,6]. However, the experimentally observed spin relaxation time $\tau_s \sim 3$ ns and spin relaxation length $\lambda_s \sim 24$ μm are [7] lower than the theoretically predicted $\tau_s \sim 100$ ns and $\lambda_s \sim 100$ μm [8,9]. There are a number of experiments and theories suggesting that the charge and magnetic impurities present in graphene might play an important role for the lower value of observed spin relaxation time [5,10–13]. It is an open question whether these impurities affect the spin transport in a similar way as the charge transport, or if the scattering mechanisms in both processes behave differently. For electronic transport in graphene, the effect of impurities can be studied via 1/f noise measurements. In a similar line, measuring low frequency fluctuations of the spin accumulation can unravel the role of impurities on the spin transport.

In this work, we report observation of spin-dependent 1/f noise, which we study on graphene spin valves performed in a nonlocal geometry. We find that the extracted noise magnitude (γ^s) for the spin transport is three orders of magnitude higher than the noise magnitude (γ^c) obtained from the local charge noise measurements, indicating different scattering mechanisms producing 1/f fluctuations in the charge and spin transport. Such a large difference had not been pointed out until now, although different scattering mechanisms for spin transport have been proposed before [11,12]. In a recent experiment, Arakawa *et al.* [14] measure a spin dependent shot noise due to the spin-injection process. Also, they rule out the effect of spin-flip scattering due to similar Fano factor values obtained for the charge and spin transport. In contrast, we measure the spin dependent noise in a different frequency regime and find out that the dominant scattering mechanisms contributing to the $1/f$ noise are the processes which flip the spins, giving rise to a higher noise magnitude compared to the charge transport and highlighting the role of impurities in the spin relaxation.

In order to perform the spin-dependent noise measurements, we prepare graphene spin valves. Single layer graphene is contacted with 35 nm thick ferromagnetic cobalt electrodes with ∼0.8 nm thick TiO_2 tunnel barrier inserted in between for efficient spin injection and detection (see Supplemental Material [15] for fabrication details) [13,16]. We characterize two different regions of our sample. They are labeled as device A and device B for further discussion.

A lock-in detection technique is used for characterizing the charge and the spin transport properties. All the measurements are carried out in high vacuum ($\sim 1 \times 10^{-7}$ mbar) at room temperature. For charge transport measurements we use the four probe connection scheme shown in Fig. 1(a), which minimizes the contribution of the contacts.

Spin transport is measured by applying a current between contacts C1-C2 to inject the spins into graphene and measure the spin accumulation between contacts C3-C5 (or C4-C5) in a four probe nonlocal detection scheme as shown in Fig. 1(b). This method decouples the paths of the spin and charge transport and thus minimizes the contribution of the charge signal to the measured spin signal [16]. In order to perform spin valve measurements, we first apply an in-plane high magnetic field ($B_\parallel$) along the easy axes of the ferromagnets to set their relative magnetization in the same direction. Then, the magnetic field is swept in the opposite direction in order to reverse the magnetization direction of the electrodes one by one depending on their coercivity. Each magnetization reversal appears as a sharp transition in the signal [Fig. 2(a)]. For Hanle precession measurements, an out of plane magnetic field ($B_\perp$)

*Corresponding author: s.omar@rug.nl

†Corresponding author: i.j.vera.marun@rug.nl

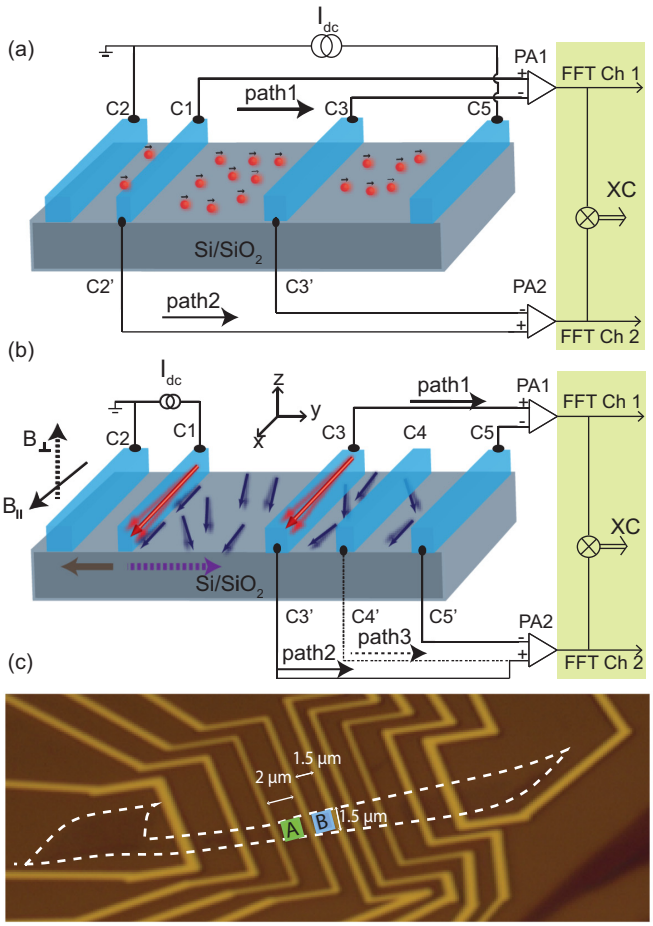

FIG. 1. (a) Cross correlation (XC) connection scheme for local charge noise measurement and (b) nonlocal spin-dependent noise measurements. A connection scheme for spatial cross correlation (SXC) is also shown where the XC analysis is performed over the voltage measured between contacts C3-C5 ($V_{\mathrm{NL}}^{C3\text{-}C5}$, path 1) and contacts C4-C5 ($V_{\mathrm{NL}}^{C4\text{-}C5(C4'\text{-}C5')}$, path 3). (c) An optical picture of the sample of single layer graphene (white dotted line) connected via FM electrodes. Noise measurements are done in two regions of the sample, labeled A ($l = 2\ \mu$m, $w = 1.5\ \mu$m) and B ($l = 1.5\ \mu$m, $w \sim 1.5\ \mu$m).

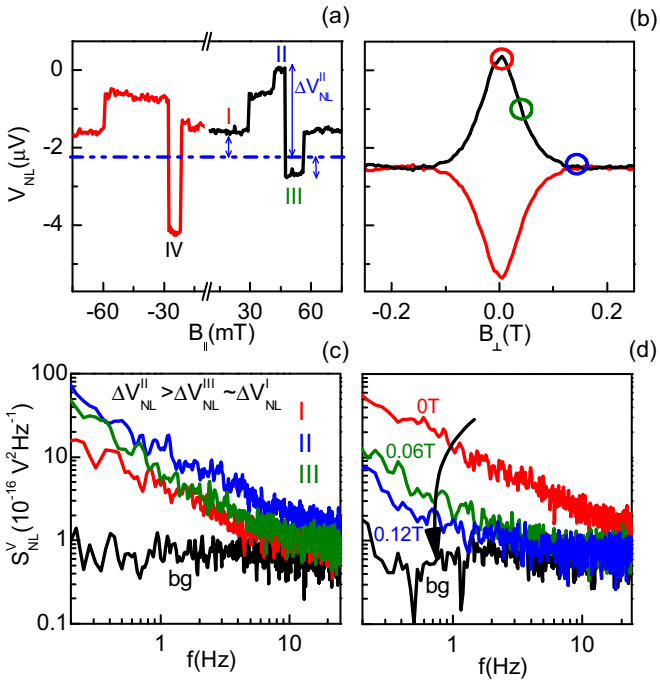

FIG. 2. (a) Nonlocal spin valve measurement. The dotted line represents the background level, which is estimated from the Hanle measurement. ΔV_{NL} is defined as the spin accumulation above or below with respect to the background level (see Supplemental Material [15] for switching details). (b) Hanle measurement is shown for the level II and level IV of the spin valve. (c) Noise PSD measured for the magnetization configurations corresponding to level I, II, and III in the spin-valve measurement in Fig. 2(a). (d) The PSD plot for the Hanle configuration obtained at different magnetic fields, corresponding to the circles indicated in Fig. 2(b). In Figs. 2(c) and 2(d), 'bg' represents the zero current background thermal noise.

is applied to precess the injected spins around the applied field for a fixed magnetization configuration of the ferromagnetic electrodes. A representative Hanle measurement from device A is shown in Fig. 2(b). With this measurement, we can extract the spin diffusion coefficient D_{s} and spin relaxation time τ_{s}, following the procedure described in Ref. [16], and use them to calculate the contact polarization (P). For device A, we obtain $D_{\mathrm{s}} \sim 0.03\ \mathrm{m}^2/\mathrm{s}$, $\tau_{\mathrm{s}} \sim 110$ ps and $P \sim 5\%$ and for device B, $D_{\mathrm{s}} \sim 0.01\ \mathrm{m}^2/\mathrm{s}$, $\tau_{\mathrm{s}} \sim 290$ ps and $P \sim 10\%$.

In order to measure the noise from the sample, we use a two channel dynamic signal analyzer from Stanford Research System (model SR785) which acquires the signal fluctuations in time and converts it into a frequency domain signal via the fast Fourier transform (FFT) algorithm.

The 1/f noise of the charge transport in graphene is measured in a local four probe scheme, similar to the charge transport measurements [Fig. 1(a)]. A dc current is applied between the ferromagnetic injectors C2 and C5. Since the contacts are designed lithographically on both sides of the ferromagnetic electrode, the fluctuations in the voltage drop V_{local} across the flake can be measured via the contact pair C1-C3 (path 1) and C1′-C3′ (path 2). The measured signals are cross correlated in order to filter out the noise from external electronics such as preamplifiers and the spectrum analyzer [17]. The electronic 1/f noise $S_{\mathrm{V}}^{\mathrm{local}}$ is measured at different bias currents (I_{dc}) at a fixed carrier density. By fitting the spectrum with the Hooge formula for 1/f noise, i.e., $S_{\mathrm{V}}^{\mathrm{local}} = \frac{\gamma^{\mathrm{c}} V_{\mathrm{local}}{}^2}{f^a}$, where V_{local} is the average voltage drop across the flake and a is the exponent $\sim$1, we obtain the noise magnitude for the charge transport $\gamma^{\mathrm{c}} \sim 10^{-7}$ [device A in Fig. 1(c)], similar to the values reported in literature [18–20] (see Supplemental Material [15] for the details). The charge noise magnitude is defined as the Hooge parameter $\gamma_{\mathrm{H}}^{\mathrm{c}}$ divided by the total number of carriers in the transport channel, i.e., $\gamma^{\mathrm{c}} = \gamma_{\mathrm{H}}^{\mathrm{c}}/(n * W * L)$. Here n is charge carrier density, and W and L are the width and length of the transport channel. γ^{c} depends both on the concentration and the type of scatterers, e.g., short range and long range scatterers [18–22].

The spin-dependent 1/f noise can be expressed as:

$$\triangle S_V^{NL} = \frac{\gamma^s \triangle V_{NL}^2}{f^a} = \frac{\gamma^s (P\mu_s/e)^2}{f^a}. \quad (1)$$

Here $\triangle S_V^{NL}$ is the spin-dependent nonlocal noise, $\gamma^s = \gamma_H^s/(n * W * \lambda_s)$ is the noise magnitude for spin transport, e is the electronic charge, and $\triangle V_{NL} = P\mu_s/e$ is the measured nonlocal spin signal due to the average spin accumulation μ_s in the channel [23]. Here γ_H^s represents the Hooge parameter for spin transport. In contrast with the charge current, spin current is not a conserved quantity and exists over an effective length scale of λ_s. Spin transport in a nonlocal geometry is realized in three fundamental steps: (i) spin current injection, (ii) spin diffusion through the transport channel, and (iii) detection of the spin accumulation. All these steps can contribute to the spin-dependent noise. For the first step of spin injection, we use a dc current source to inject spin current, which helps to eliminate the resistance fluctuations in the injector contact, leaving only the polarization fluctuations of the injector electrode as a possible noise source. The polarization fluctuations of the injector can arise due to thermally activated domain wall hopping/rotation in the ferromagnet [24,25]. The second possible noise source contributing to the fluctuations in the spin accumulation is the transport channel itself, either via the fluctuating channel resistance or via fluctuations in the spin-relaxation process. The third noise source, similar to the first one, can be present at the detector electrode due to fluctuating contact polarization.

The spin-dependent noise in graphene is measured nonlocally as shown in the connection diagram of Fig. 1(b). During the noise measurement, we keep the spin injection current I_{dc} fixed (10 μA) and change the detected spin accumulation in three different ways. At $B_\perp = 0$ T, (i) by changing the spin accumulation by switching the relative magnetization direction of the injector electrodes, (ii) by keeping the spin accumulation constant and changing the spin detection sensitivity by switching the relative magnetization direction of detector electrodes, and (iii) at $B_\perp \neq 0$ T, by dephasing the spins during transport and thus reducing the spin accumulation. We can also measure the noise due to a spin independent background signal at high $B_\perp \sim 0.12$ T, where the spin accumulation is suppressed. The spin-dependent component $\triangle S_V^{NL}$ can be estimated by subtracting S_V^{NL} (at $B_\perp \sim 0.12$ T) from the measured S_V^{NL}.

For the nonlocal noise measurements in spin valve configuration, the noise PSD measured [Fig. 2(c)] for the magnetization configuration corresponding to a higher spin accumulation (level II; blue spectrum) is higher in magnitude than for the one corresponding to a lower spin accumulation (level I; red spectrum) of the spin valve in Fig. 2(a). In a similar way for the Hanle configuration, we measure the maximum magnitude of the spin-dependent noise for $B_\perp = 0$ T, corresponding to maximum spin accumulation [Fig. 2(d)]. On increasing $|B_\perp|$, both the spin accumulation and the associated noise are reduced. In order to study its dependence with the spin accumulation, we fit each measured spectrum of S_V^{NL} versus frequency, obtained at different spin accumulation values ($\triangle V_{NL}$) with Eq. (1) in the frequency range of 0.5–5 Hz. We take the value of S_V^{NL} at $f = 1$ Hz from the fit as a representative value of the 1/f spectrum.

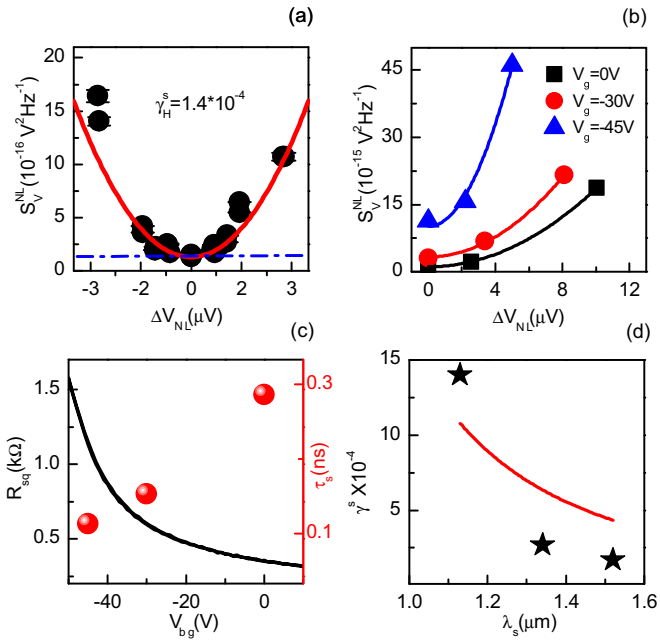

FIG. 3. (a) Summary of noise measured for different spin accumulation potentials in Hanle configuration (device A) and the parabolic fit for the data (red line) using Eq. (1). Here blue dotted line denotes the spin independent charge noise background, i.e., S_V^{NL} (at $B_\perp \sim 0.12$ T). (b) Spin dependent 1/f noise in Hanle configuration, measured as a function of back-gate voltage (device B). The increased background noise at $\triangle V_{NL} = 0$ V can come from the charge noise contribution to the nonlocal signal ($S_{1/f}^V \propto I^2 {R_{sq}}^2$). (c) The graphene sheet resistance increases at negative back-gate voltage reflecting the n-type doping in graphene and the spin relaxation time (red circles) decreases at lower carrier density for the single layer graphene, resulting in lower value for λ_s. (d) γ^s is increased for lower value of $\lambda_s(\tau_s)$ (black stars), indicating the influence of the spin-flip processes on the extracted noise magnitude for spin transport. A plot of γ^s versus λ_s with Eq. (2) (red curve) shows similar behavior. For the plot, we assume the polarization noise (offset) to be zero, the values for $L = 1.5$ μm, and $S_{\lambda_s} \sim 10^{-16}$ m^2 Hz^{-1}.

The exponent a obtained from the fit is ~ 1. A summary of the data points for the noise PSD at different values of spin accumulation, obtained for device A using Hanle precession, is plotted in Fig. 3(a). The $\triangle S_V^{NL} \propto {\mu_s}^2$ relation is valid in the lowest order approximation. The parabolic fit of the measured nonlocal noise using Eq. (1) gives $\gamma^s \sim 10^{-4}$. It should be noted that $\gamma^s \sim 1000 \times \gamma^c$, for the same device. Geometrical factors such as length scales cannot account for such a huge difference, as for this sample we obtain $\lambda_s \sim 1.5\,\mu$m which is similar to the channel length for charge 1/f noise. The three orders of magnitude enhanced γ^s points towards distinctive scattering processes affecting the spin dependent noise, in contrast to the charge 1/f noise. Our findings can be explained along the direction of the recently proposed resonant scattering mechanism [11] for spin transport where intrinsically present magnetic impurities strongly scatter the spins without a significant effect on the charge scattering strength. The scattering cross section of these impurities can fluctuate in time and could give rise to a spin dependent 1/f noise.

An analytical expression for the spin-dependent noise (at $f = 1$ Hz) which is derived from the equation for the nonlocal spin signal $\triangle V_{\mathrm{NL}}$ (see Supplemental Material [15] for the complete derivation) can be written as:

$$\frac{\triangle S_V^{\mathrm{NL}}}{\triangle V_{\mathrm{NL}}^2} = \gamma^{\mathrm{s}} \simeq \frac{S_P}{P^2} + \frac{S_{\lambda_{\mathrm{s}}}}{{\lambda_{\mathrm{s}}}^2}\left(1 + \frac{L}{\lambda_{\mathrm{s}}}\right)^2, \tag{2}$$

where S_P is the contact polarization noise which is Fourier transform of the auto correlation function for the time dependent polarization fluctuations, i.e., $\mathcal{F}\langle P(t)P(t+\tau)\rangle$, $S_{\lambda_{\mathrm{s}}}$ is the noise associated with the spin transport, i.e., spin relaxation noise ($\mathcal{F}\langle\lambda_{\mathrm{s}}(t)\lambda_{\mathrm{s}}(t+\tau)\rangle$), and L is the separation between the inner injector and detector electrodes. Equation (2) suggests that γ^{s} is increased for lower values of λ_{s}. In order to confirm that the spin-dependent noise is affected by the spin transport properties, we measure $S_{\mathrm{V}}^{\mathrm{NL}}$ as a function of the back-gate voltage (carrier density). In agreement with literature [26,27], a higher τ_{s} is observed at higher charge carrier densities for single layer graphene [Fig. 3(c)]. The representative data is shown for device B. It is worth emphasizing here that for similar charge and spin transport parameters (R_{sq},λ_{s}) for device A (350 Ω, 1.8 μm) and device B (400 Ω, 1.6 μm), we obtain similar values of $\gamma^{\mathrm{s}} \sim 10^{-4}$. However, both devices have different values of contact polarization $P \sim 5\%$ for device A and $P \sim 10\%$ for device B. This similarity in γ^{s} values despite the difference in P indicates that there is insignificant contribution of the contact polarization noise to the extracted γ^{s}. On the other hand, for the noise measurements at different carrier densities, we get an increase in γ^{s} at lower values of τ_{s} [Fig. 3(d)]. The carrier density dependent behavior of the extracted γ^{s} is in qualitative agreement with the λ_{s} dependence of γ^{s} in Eq. (2) [red curve in Fig. 3(d)], supporting our hypothesis that the measured spin-dependent noise is dominated by the noise produced by the spin transport (relaxation) process in graphene.

In order to estimate/filter out the contribution of the contact polarization noise in our measurements, we use spatial cross-correlation (SXC). We measure the contact polarization noise ($=S_P/P^2 \times \triangle V_{\mathrm{NL}}^2 \sim 10^{-16}\mathrm{V}^2\,\mathrm{Hz}^{-1}$) which is lower by two orders of magnitude than the spin relaxation noise power between C3 and C5 ($=S_{\lambda_{\mathrm{s}}}/{\lambda_{\mathrm{s}}}^2 \times \triangle V_{\mathrm{NL}}^2 \sim 10^{-14}\mathrm{V}^2\,\mathrm{Hz}^{-1}$) (see Supplemental Material [15] for measurement scheme). Here, based on the reciprocity argument for the injector and detector in spin-valve configuration, we can assume equal noise contribution from the injector electrode and can safely rule out the effect of the polarization noise.

Since the spin accumulation $\mu_{\mathrm{s}} \propto \exp^{(-L/\lambda_{\mathrm{s}})}$, the spin relaxation noise is also expected to decay exponentially in accordance with the relation $\triangle S_{\mathrm{V}}^{\mathrm{NL}} \propto {\mu_{\mathrm{s}}}^2$. We extend our analysis to study the distance dependence of the spin relaxation noise. With the spatial cross-correlation we can also measure the spin relaxation noise between the detector contacts C4 and C5 while removing the polarization noise from contact C4. For this, we measure the spin-dependent noise at different detector contacts via path 1 and path 3 in Fig. 1(b) independently, and cross correlate the measured signals (see Supplemental Material [15]). The polarization noise contribution from the reference detector C5 is expected to be negligible due to the lower value of spin accumulation at the contact ($L_{\mathrm{C1\text{-}C5}}/\lambda_{\mathrm{s}} \sim 4$). We measure $\triangle S_{\mathrm{V}}^{\mathrm{NL}}$ at the detectors C3 and C4 for two back-gate voltages: at $V_{\mathrm{g}} = 0$ V (metallic regime) and at $V_{\mathrm{g}} = -45$ V (close to the Dirac point) (see Supplemental Material [15]). Using the derived Eq. (2), we can now calculate λ_{s} from the noise measurement as:

$$\frac{S_{\lambda_{\mathrm{s}}}^{\mathrm{C3}}}{S_{\lambda_{\mathrm{s}}}^{\mathrm{C4}}} \simeq \left(\exp\frac{L^{C3-C4}}{\lambda_{\mathrm{s}}}\right)^2 \left(\frac{1 + \frac{L^{\mathrm{C1\text{-}C3}}}{\lambda_{\mathrm{s}}}}{1 + \frac{L^{\mathrm{C1\text{-}C4}}}{\lambda_{\mathrm{s}}}}\right)^2. \tag{3}$$

Here $S_{\lambda_{\mathrm{s}}}^{\mathrm{C3}}$ and $S_{\lambda_{\mathrm{s}}}^{\mathrm{C4}}$ are the spin relaxation noise at contacts C3 and C4, and L^{Ci-Cj} is the separation between contacts C_i and C_j ($i,j = 1,3,4$). The solution to Eq. (3) for the experimentally obtained noise ratios gives a value of $\lambda_{\mathrm{s}} \sim 1.5$ μm and 1.0 μm at $V_{\mathrm{g}} = 0$ V and -45 V, respectively. A close agreement with the values obtained independently from the Hanle measurements ($\lambda_{\mathrm{s}} \sim 1.5$ μm at $V_{\mathrm{g}} = 0$ V and 1.1 μm at $V_{\mathrm{g}} = -45$ V) validates the analytical framework of Eqs. (2) and (3).

By performing the first measurement of 1/f noise associated with spin transport, we demonstrate that the nonlocal spin-dependent noise in graphene is dominated by the underlying spin relaxation processes. The obtained noise magnitude for charge and spin transport differs by three orders of magnitude, indicating fundamentally different scattering mechanisms such as resonant scattering of the spins, where the fluctuating scattering cross section of the intrinsically present impurities could produce the spin dependent 1/f fluctuations [11]. The presented work establishes 1/f noise measurements as a complementary approach to extract spin transport parameters and is expected to be valid for other spintronic materials, where impurities play an important role in modifying the underlying spin relaxation process.

We acknowledge J. G. Holstein, H. M. de Roosz, and H. Adema for their technical assistance. This research work was financed under EU-graphene flagship program (637088) and supported by the Zernike Institute for Advanced Materials, Nederlandse Organisatie voor Wetenschappelijk (NWO, Netherlands) and the Future and Emerging Technologies (FET) programme within the Seventh Framework Programme for Research of the European Commission, under FET-open Grant No. 618083 (CN-TQC).

[1] R. Landauer, Nature (London) **392**, 658 (1998).

[2] R. Jayaraman and C. Sodini, IEEE Trans. Electron Devices **36**, 1773 (1989).

[3] F. N. Hooge, T. G. M. Kleinpenning, and L. K. J. Vandamme, Rep. Prog. Phys. **44**, 479 (1981).

[4] P. Dutta and P. M. Horn, Rev. Mod. Phys. **53**, 497 (1981).

[5] C. Ertler, S. Konschuh, M. Gmitra, and J. Fabian, Phys. Rev. B **80**, 041405 (2009).

[6] D. Huertas-Hernando, F. Guinea, and A. Brataas, Phys. Rev. Lett. **103**, 146801 (2009).

[7] J. Ingla-Aynés, M. H. D. Guimarães, R. J. Meijerink, P. J. Zomer, and B. J. van Wees, Phys. Rev. B **92**, 201410 (2015).

[8] V. K. Dugaev, E. Y. Sherman, and J. Barnaś, Phys. Rev. B **83**, 085306 (2011).

[9] H. Min, J. E. Hill, N. A. Sinitsyn, B. R. Sahu, L. Kleinman, and A. H. MacDonald, Phys. Rev. B **74**, 165310 (2006).

[10] M. B. Lundeberg, R. Yang, J. Renard, and J. A. Folk, Phys. Rev. Lett. **110**, 156601 (2013).

[11] D. Kochan, M. Gmitra, and J. Fabian, Phys. Rev. Lett. **112**, 116602 (2014).

[12] D. Soriano, D. V. Tuan, S. M.-M. Dubois, M. Gmitra, A. W. Cummings, D. Kochan, F. Ortmann, J.-C. Charlier, J. Fabian, and S. Roche, 2D Mater. **2**, 022002 (2015).

[13] S. Omar, M. Gurram, I. J. Vera-Marun, X. Zhang, E. H. Huisman, A. Kaverzin, B. L. Feringa, and B. J. van Wees, Phys. Rev. B **92**, 115442 (2015).

[14] T. Arakawa, J. Shiogai, M. Ciorga, M. Utz, D. Schuh, M. Kohda, J. Nitta, D. Bougeard, D. Weiss, T. Ono, and K. Kobayashi, Phys. Rev. Lett. **114**, 016601 (2015).

[15] See Supplemental Material at http://link.aps.org/supplemental/10.1103/PhysRevB.95.081403 for the charge 1/f noise measurements, additional spin dependent non-local noise measurements, an analytical derivation of spin dependent noise and a two channel resistor model for thermal and 1/f noise analysis. It also includes the spatial cross correlation measurements for the polarization noise and the spin-relaxation noise.

[16] N. Tombros, C. Jõzsa, M. Popinciuc, H. T. Jonkman, and B. J. van Wees, Nature (London) **448**, 571 (2007).

[17] H. E. van den Brom and J. M. van Ruitenbeek, Phys. Rev. Lett. **82**, 1526 (1999).

[18] A. A. Balandin, Nat. Nano **8**, 549 (2013).

[19] A. N. Pal, S. Ghatak, V. Kochat, E. S. Sneha, A. Sampathkumar, S. Raghavan, and A. Ghosh, ACS Nano **5**, 2075 (2011).

[20] G. Liu, S. Rumyantsev, M. S. Shur, and A. A. Balandin, Appl. Phys. Lett. **102**, 093111 (2013).

[21] A. A. Kaverzin, A. S. Mayorov, A. Shytov, and D. W. Horsell, Phys. Rev. B **85**, 075435 (2012).

[22] M. A. Stolyarov, G. Liu, S. L. Rumyantsev, M. Shur, and A. A. Balandin, Appl. Phys. Lett. **107**, 023106 (2015).

[23] Variables V_{local}, $\triangle V_{\text{NL}}$, μ_s, P, λ_s represent the time average of the quantities.

[24] L. Jiang, E. R. Nowak, P. E. Scott, J. Johnson, J. M. Slaughter, J. J. Sun, and R. W. Dave, Phys. Rev. B **69**, 054407 (2004).

[25] S. Ingvarsson, G. Xiao, R. A. Wanner, P. Trouilloud, Y. Lu, W. J. Gallagher, A. Marley, K. P. Roche, and S. S. P. Parkin, J. Appl. Phys. **85**, 5270 (1999).

[26] P. J. Zomer, M. H. D. Guimarães, N. Tombros, and B. J. van Wees, Phys. Rev. B **86**, 161416 (2012).

[27] C. Jõzsa, T. Maassen, M. Popinciuc, P. J. Zomer, A. Veligura, H. T. Jonkman, and B. J. van Wees, Phys. Rev. B **80**, 241403 (2009).